A comparison of open versus closed loop flexure compensation systems for two Keck optical imaging spectrographs: ESI and DEIMOS

Robert Kibrick, S. M. Faber, Andrew C. Phillips, Molly McVeigh, Dave Cowley, Matt Radovan, Kirk Gilmore, Chris Wright, Dean Tucker, De Clarke, Steve Allen

UCO/Lick Observatory, University of California, Santa Cruz, California 95064 USA

ABSTRACT

Two recent Keck optical imaging spectrographs have been designed with active flexure compensation systems (FCS). These two instruments utilize different methods for implementing flexure compensation.

The Echellette Spectrograph and Imager (ESI), commissioned at the Cassegrain focus of the Keck II Telescope in late 1999, employs an open-loop control strategy. It utilizes a mathematical model of gravitationally-induced flexure to periodically compute flexure corrections as a function of telescope position. Those corrections are then automatically applied to a tip/tilt collimator to stabilize the image on the detector.

The DEep Imaging Multi-Object Spectrograph (DEIMOS), commissioned at the Nasmyth focus of Keck II in June 2002, implements a closed-loop control strategy. It utilizes a set of fiber-fed FCS light sources at the ends of the slitmask to produce a corresponding set of spots on a pair of FCS CCD detectors located on either side of the science CCD mosaic. During science exposures, the FCS detectors are read out several times per minute to measure any translational motion of the FCS spot images. Correction signals derived from these FCS images are used to drive active optical mechanisms which steer the spots back to their nominal positions, thus stabilizing the FCS spot images as well as those on the science mosaic.

We compare the design, calibration, and operation of these two systems on the telescope. Long-term performance results will be provided for the ESI FCS, and preliminary results will be provided for the DEIMOS FCS.

Keywords: active flexure compensation, spectrograph flexure, DEIMOS, ESI

1. INTRODUCTION

As pointed out by Walker and D'Arrigo,[1] flexure within spectrographs results in image motion at the detector which reduces spectral and spatial resolution, degrades line profiles and radial velocities, and induces misalignment of flat fields. Such image motion requires observers to regularly obtain calibration arc spectra and flat fields at representative telescope positions during observing, thereby wasting significant amounts of telescope time. While flexure might be reduced to acceptable levels using a carefully-tuned passive mechanical design,[2,3] they argue that reasonable constraints on mass, space, and cost may preclude such a solution, and that some form of active flexure compensation may prove more practical.

In the past 5 years, active flexure compensation systems have been included in the designs for several large optical spectrographs, including the High Resolution Optical Spectrograph (HROS)[4] and Gemini Multi-object Spectrograph (GMOS)[5] for the Gemini Telescopes, the Multi-object Spectrograph and Imager (IMACS)[6] for the Magellan I Telescope, and the ESI[7] and DEIMOS[8] spectrographs for the Keck II Telescope. Given the success of this approach, we anticipate that active FCS will be a standard component of future large optical spectrographs.

Further author information- (Send correspondence to R.K)
R.K.: Email: kibrick@ucolick.org; http://www.ucolick.org/~kibrick; Telephone: 831-459-2262; Fax: 831-459-2298;
S.F.: Email: faber@ucolick.org; Telephone: 831-459-2944; D.P.: Email: phillips@ucolick.org; Telephone: 831-459-2476;
M.R.: Email: mvr@ucolick.org; Telephone: 831-459-2557; K.G.: Email: gilmore@ucolick.org; Telephone: 831-459-3184;
C.W.: Email: cwright@ucolick.org; Telephone: 831-459-2835; D.T.: Email: tucker@ucolick.org; Telephone: 831-459-4903; D.C.: Email: de@ucolick.org; Telephone: 831-459-2630; S.A.: Email: sla@ucolick.org; Telephone: 831-459-3046

2. THE ESI SPECTROGRAPH OPEN-LOOP FCS

2.1. Overview

The ESI spectrograph has three operating modes: direct imaging, low-resolution, and echellette. Using a set of movable mirrors and prisms (each of which can be moved in or out of the light path), the collimated beam can be directed either to the camera for imaging, through a prism disperser, or to an echellette grating with prism cross-dispersion.

ESI compensates for gravitationally-induced flexure via its collimator mirror. The collimator has three actuators that are moved in tandem to adjust collimator focus, while individual offsets can be applied to each actuator to adjust tip and tilt. The ESI FCS software utilizes a mathematical model of gravitationally-induced flexure to periodically compute and apply flexure corrections by commanding the corresponding tip and tilt motions to the collimator.[9] A separate flexure model is used for each of the three instrument modes (echellette, low-dispersion, and imaging.) Although the flexure model is recalculated at a 1 Hz rate, corrections are not applied until the accumulated image motion reaches 0.1 pixel in magnitude so as to avoid unnecessary use of the collimator actuators. All three actuators are updated in parallel to minimize response time and mechanical stress on the collimator mechanism.

The ESI FCS only compensates for those errors which can be modeled in terms of gravity-driven flexure. Non-modeled errors include those that result from changes in temperature across the instrument structure, from lost motion in optical stages and in the camera, and from small zero point shifts that are observed whenever the instrument is removed from and then re-inserted into the telescope. In addition, there is out-of-roundness or runout between the instrument and the rotator module. While the determinate structure that attaches ESI to the Cassegrain rotator module isolates most of the bearing stresses from the instrument, a small amount of residual stress contributes to the observed hysteresis and image motion. Image motions induced by such stresses are neither modeled nor corrected by our model of gravitationally-induced flexure.

The first operational test of the ESI FCS system took place during instrument commissioning at the Mauna Kea summit in September 1999. The flexure model was refined during subsequent engineering runs in October and November. The system became operational for science observing at the end of 1999 and is now in routine use. Image motion due to flexure has been reduced by a factor of ten to a few tenths of a pixel (or about 0.04 arc-seconds on the sky) for a typical exposure.

2.2. Modeling

Measurements of image motion versus collimator motion were obtained in all three instrument modes to determine the relevant transformations and to verify that the system operated linearly. However, due to anamorphic distortion from the two cross dispersing prisms in the two spectroscopic modes, the effective gain of the collimator actuators is not constant across the detector. In order to simplify the control algorithm, a specific image feature near the center of the detector was selected as the central reference for each instrument mode. The gain for each actuator were then determined for each instrument mode using its respective reference feature. These same reference features were later used when measuring the image motions induced by spectrograph flexure. These measurements were obtained with the instrument and rotator module installed in the Keck II Telescope.

Gravitational flexure in ESI was modeled using a linear elasticity model for fitting the image motion versus spectrograph position data:

$$X(\phi,\, \theta) = a_0 + a_1 \cos\phi \cos\theta + a_2 \cos\phi \sin\theta + a_3 \sin\phi \tag{1}$$

$$Y(\phi,\, \theta) = b_0 + b_1 \cos\phi \cos\theta + b_2 \cos\phi \sin\theta + b_3 \sin\phi, \tag{2}$$

where X corresponds to the predicted position of the reference feature in the X (or column) axis of the CCD, Y to the predicted position in the Y (row) axis, ϕ to the telescope elevation angle, θ to the rotator physical angle, and a_i and b_i are the corresponding coefficients obtained from a least square fit of the data to the model. Each instrument mode is fitted separately.

The gravitational flexure model provided a relatively good fit to the observed data for all three modes. Worst-case and rms residuals for each mode were, respectively: imaging 0.63 and 0.29 pixels, low-resolution

0.66 and 0.25 pixels, echellette 0.64 and 0.25 pixels. The ESI CCD detector has 15 micron pixels and the plate scale is 0.153 arc-seconds per pixel. Accordingly, the worst-case residuals and rms residuals were about 0.1 and 0.04 arc-seconds on the sky.

2.3. Initial Results

Measurements of image motion induced by spectrograph flexure were obtained with the instrument and rotator module installed in the Keck II telescope. Calibration spectra were obtained in the two spectroscopic modes by illuminating a pinhole adjacent to the echellette slit with the various line lamps. Images of this pinhole were also obtained in imaging mode. The telescope was stepped in elevation between 0°, 30°, 60° and 90°. At each of these four elevations, calibration data were obtained at 17 different rotator position angles, sampling two full revolutions (one clockwise, one counterclockwise) in increments of 45° rotation. All flexure measurements for each mode were made using the same central reference features as were used to calibrate the actuator gains. The results of the flexure measurements obtained during the 1999 October engineering run are shown for the echellette mode in Figs. 1 and 2. The results for the other two modes are similar. Note that in echellette mode the dispersion direction is parallel to the columns (or Y-axis).

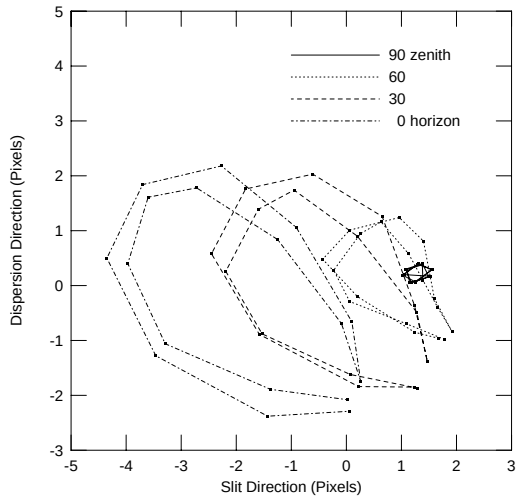

Figure 1. Echellette mode flexure map

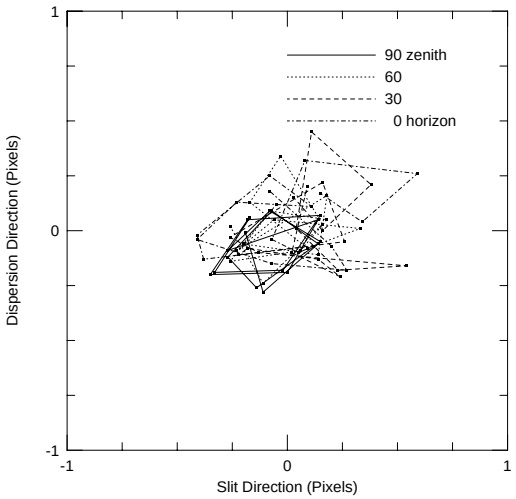

Figure 2. Echellette mode residual-flexure

2.4. Long Term Results

The long term stability of the FCS calibration has been measured by comparing the echellette mode flexure models that were derived from flexure calibrations performed in October and November 1999 with those obtained from a pair of calibrations conducted on the same night in March 2001. While some large zero point shifts (the a_0 and b_0 terms) were observed when comparing the 2001 calibrations to those performed in 1999, these were most likely the result of an adjustment to the dewar position performed in January 2000. However, the zero point stability over the course of one night is about 0.15 pixel. Thus, one can compensate for any longer-term zero point shifts by taking a single calibration exposure at the start of a night and adjusting the FCS operational zero point accordingly.

While the values of the angularly dependent model coefficients (a_1, a_2, a_3, and b_1, b_2, b_3) varied by as much as 20% from one calibration model to the next, the models they represent agree quite closely, once the respective zero points are aligned. Predicted image positions from each of the four models produced by these calibrations were compared. The worst-case differences observed between corresponding positions were 0.43 pixel in X and 0.24 pixel in Y, while the rms errors across all four models were 0.11 pixel in X and 0.07 pixels in Y.

On the basis of these results, and assuming that no significant mechanical or optical modifications are made to the instrument, a given flexure calibration model can be expected to provide acceptable FCS performance for at least one year. Thus, aside from nightly checks of the FCS zero point, frequent re-calibration of the flexure model is not needed to maintain FCS performance.

3. THE DEIMOS SPECTROGRAPH CLOSED-LOOP FCS

3.1. Overview

The Deep Imaging Multi-Object Spectrograph (DEIMOS), located at the right Nasmyth focus of the Keck II telescope, is a general purpose, faint-object, multi-slit spectrograph whose key features are wide spectral coverage, high spectral resolution, high throughput, and long slit length on the sky. The instrument is housed in a cylindrical enclosure which rotates to counteract the field rotation inherent in an alt-az telescope.

DEIMOS operates in three modes: direct imaging, single-object spectroscopy, and multi-object spectroscopy. For spectroscopy, a remotely-operable slit mask mechanism enables rapid insertion of and switching between a single longslit mask and up to ten multi-slit masks, while for direct imaging the mechanism retracts all masks from the optical path. Unlike ESI, which implements its multiple operating modes using a movable prism and flat mirror, and a single, fixed-position, non-tiltable grating, DEIMOS offers a choice of gratings and grating tilts via three movable mechanisms, called sliders. One slider holds the mirror used for direct imaging and the other two hold the gratings used for spectroscopy; the former operates at a fixed tilt while each of the latter includes a precision grating tilt mechanism capable of tilting a grating through an angle of nearly 40 degrees. Each of the two grating sliders can accept several different grating cells, but removal and insertion of grating cells is a manual process performed during the daytime. Four cells are currently loaded with gratings of varying ruling densities: 600, 830, 900, and 1200 grooves/mm. (The grating dispersion varies from 0.325 Å/px for the 1200 grooves/mm grating to 0.65 Å/px for the 600. The plate scale is 0.119 arc-seconds/px and the pixels are 15 by 15 microns.)

A remotely-controlled mechanism enables astronomers to switch between the different sliders during observing. Each slider is carried by a common leadscrew that is used to drive the selected slider into the optical path. Once so positioned, the selected slider is kinematically clamped to a mounting box via a series of pneumatically-operated clamps. The time required to change between sliders varies between 2 and 3 minutes depending on their relative positions along the leadscrew.

A closed-loop approach was chosen for the DEIMOS FCS (as opposed to the open-loop approach used in ESI) because of the significantly greater number and complexity of its moving parts, the variety of gratings and tilts over which they would be used, and the stringent image motion requirements (see Sect. 3.2) imposed by the desire to control flat-fielding errors. DEIMOS utilizes a set of fiber-fed FCS light sources at the ends of the slitmask to produce a corresponding set of spots on a pair of FCS CCD detectors located on either side of the science CCD mosaic (see Fig. 3). During science exposures, the FCS detectors are read out several times per minute to measure any translational motion of the FCS spot images. Correction signals are derived from these FCS images and used to drive active optical mechanisms which steer the spots back to their nominal positions, thus stabilizing the FCS spot images as well as those on the science mosaic (see Fig. 4).

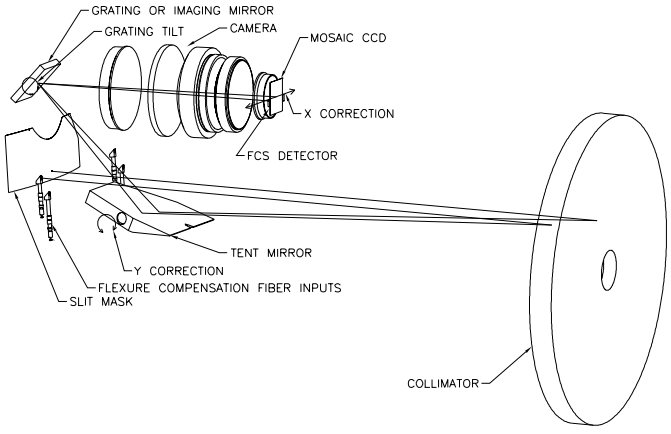

Figure 3. Optical overview of DEIMOS FCS

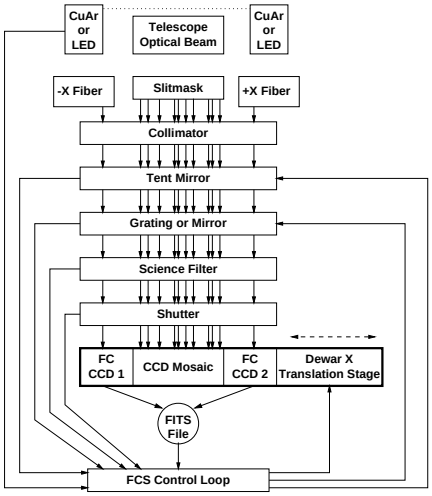

Figure 4. Block diagram of DEIMOS FCS

The DEIMOS FCS is designed to maintain constant image position on the detector over short time scales as the spectrograph rotates, and over longer time scales between the afternoon flat-field calibrations and evening observing. As position angle changes, flexural deformation of the optical supports causes image motion on the detector, while additional image motion is caused by imperfect re-positioning of the optical elements. Most important are the gratings, which are frequently moved as sliders are repositioned during an observing run or whenever the grating complement is manually altered prior to a run.

DEIMOS compensates for these short and long time scale motions via a tiltable tent mirror, which steers the image in the DEIMOS Y coordinate (along the spectrum), and a translation stage within the dewar, which moves the position of the science CCD mosaic in the DEIMOS X coordinate (along the slit). In addition, when operating in spectroscopic mode, the image can also be steered in Y using the grating tilt mechanism of the selected slider; this is necessary whenever the image motion in that axis demands a correction that exceeds the operating range of the tent mirror. This extra compensation range in Y is not available in direct imaging mode, since the slider that holds the imaging flat mirror holds it at a fixed tilt.

Like ESI, the DEIMOS FCS can only compensate for image translation errors and cannot compensate for image motion due to rotation or changes in image scale. However, unlike ESI, which can only compensate for translation errors that can be modeled in terms of gravity-driven flexure, the DEIMOS FCS is able to compensate for such errors that result from other sources, such as temperature change across the instrument, mechanical hysteresis in moving mechanisms or in camera cell supports, or zero point shifts due to slider re-positioning errors or grating cell re-insertion errors. In addition, because DEIMOS has FCS CCDs located on either side of the science CCD mosaic, it can measure and report both image rotation and changes in image scale even if it cannot correct for them. The ability to detect a change in image scale is an important diagnostic for monitoring the performance of the thermal compensators in the DEIMOS camera; those compensators are designed to minimize scale changes that can result from a temperature-induced change in the spacing between camera elements.

The first operational test of the DEIMOS FCS system took place during instrument commissioning at the Mauna Kea summit in June 2002. The FCS control loop was refined during the next engineering run in July, but considerable work remains to optimize its performance. Preliminary results indicate that image motion has been reduced by a factor of 50 to about 0.4 pixel for a typical exposure.

3.2. Specifications

The inclusion of an FCS in DEIMOS was driven mainly by the desire to control flat-fielding errors by ensuring that the wavelength of light falling on a given CCD pixel remains constant for a given configuration of the spectrograph. A secondary goal was to maintain image quality. Thus, two types of image stability are required, each with its own timescale:

3.2.1. Maintaining constancy of wavelength on a pixel

We wish to keep the spectrum tightly locked in the direction parallel to dispersion, but displacements perpendicular to the dispersion can be larger. In the dispersion direction, the original image stability goal ws ± 0.25 px. This arose from a flat-fielding accuracy requirement of 0.2% together with a certain projected fringing amplitude and fringe-phase cycle length. The actual red-sensitive CCDs from MIT/Lincoln Laboratory have a short cycle length of 24 Å but fringing amplitude of only $\pm 2\%$. This translates to a pixel stability requirement of ± 0.6 px, or about a factor of two looser than the original specification. The need is to keep the flat-field calibration and the object spectrum aligned, so this tolerance must be met over a night at least, and longer if flat-field calibrations are to be long-lived.

Displacements that are exactly parallel to the slit (i.e., following the slit curvature) have no effect on the wavelength of the illuminating light, and technically *no* specification is needed to limit the effect of such displacements. However, the actual stability specifications are stated in terms of rectilinear coordinates along and perpendicular to dispersion. A purely vertical (perpendicular) motion of the detector follows the slit closely near the middle but not at the top and bottom, due to slit curvature. Let $t = \delta y/\delta x$ describe the local tilt of the slit. The specification on the allowed vertical displacement of the spectrum in pixels is then $0.25t^{-1}$, where t is the minimum value obtained over the image.

3.2.2. Maintaining image quality

Again, there are two requirements: one along the slit, which affects angular resolution on the sky, and one perpendicular to the slit, which affects wavelength resolution. In practice, they are comparable, and we shall set them equal to a 1-px (0.119 asec) total smear *during an exposure*, or ± 0.5 px (± 0.060 asec) relative to the center of an exposure. The image quality specification is slightly easier than the wavelength-constancy specification, though of comparable size, and it lasts over only a single exposure.

The DEIMOS position angle will in general vary by up to 360° during a night, and, because Keck is an alt-az telescope, by up to 180° during a single exposure. The image stability specifications must therefore be met through a 180° rotation, while the wavelength stability specifications must be met through all position angles.

3.3. Hardware Components

3.3.1. FCS fibers and light sources

The FCS fibers and light sources are used to generate a set of artificial objects in the focal plane. A set of optics at the telescope focal-plane-end of each fiber produces an output cone at f/15 so as to match the f/ratio of the output beam from the telescope. Four 200 micron core fibers are used, with two fibers mounted to the $-X$ edge of the slitmask and the other two to the $+X$ edge (see Fig. 5). The pair of fibers on each edge are nearly centered along the Y axis but are slightly offset from one another in Y (the dispersion axis) so that the spectra they generate are offset in wavelength. Each fiber is mounted to an alignment mechanism that allows the fiber end to be positioned precisely in 3 axes. Tip and tilt adjustment is provided to correctly position the pupil on the grating. Each fiber can also be positioned to focus its spots on the detector. The focus adjustment places the end of the folded fiber image on the cylindrical surface defined by the slit mask.

The far end of each fiber is illuminated by one of two remotely controlled light sources: a CuAr arc lamp or a white light LED (all four fibers are illuminated with the same light). The CuAr lamp produces a rich spectrum with broad wavelength coverage (see Fig. 6), and can be used in either spectroscopic or direct-imaging modes. The LED can be used whenever the currently-selected science filter renders the CuAr lamp too bright for use in direct imaging mode. (The light emitted from the ends of the FCS fibers travels through all the same optical elements as the light that passes through the slits in the slitmask, so the intensity of FCS light that reaches the FCS CCDs depends on the transmission characteristics of the currently selected filter and grating.) Both light sources are mounted in the enclosed electronics ring at the far end of the instrument, where any heat they generate can be removed via the observatory's glycol cooling facility.

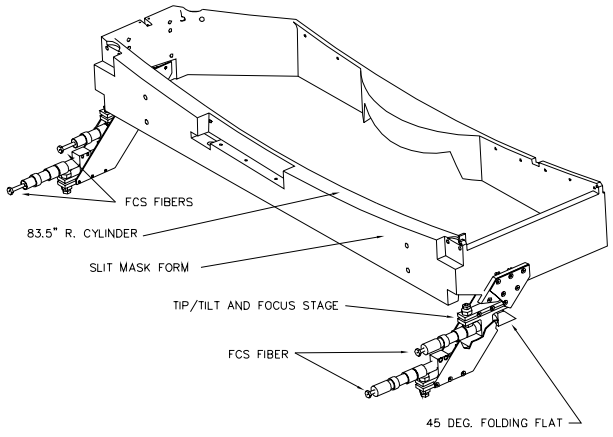

Figure 5. FCS fiber attachments to slitmask form

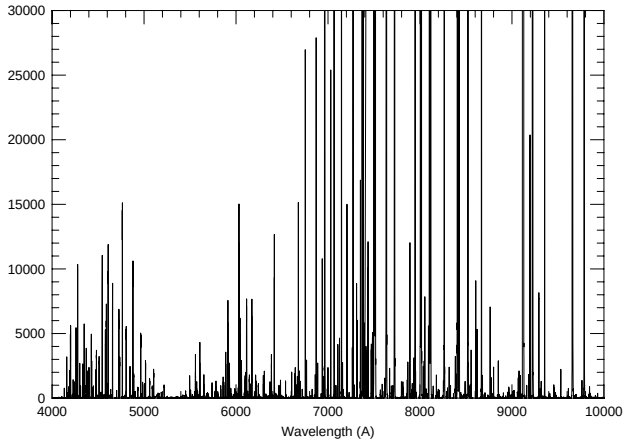

Figure 6. Spectrum of CuAr light source

3.3.2. Tent mirror

The tent mirror receives the output beam from the collimator and reflects it onto either a grating or the direct imaging mirror (see Fig. 3). The tent mirror pivots in one axis and is used to steer the image in DEIMOS *Y* (spectral direction). We decided to use the tent mirror for this task, instead of using a separate Y-translation stage in the dewar, because it was mechanically simpler. The tent mirror is driven by a Physik Instrument (PI) P845.60 low-voltage piezoelectric actuator that has a stroke of 90 microns. The actuator assembly contains a strain gauge sensor (with 10 nm resolution) for position feedback, enabling the PI controller to provide linear operation of the actuator and repeatability to within 0.1%. The actuator and the tent mirror mechanism exhibit negligible backlash and enable steering of the image to better than 0.01 pixel on both the science mosaic the and FCS CCDs.

Due to anamorphic magnification in the spectrograph, the range over which the tent mirror can steer the image varies by a factor of 1.8 depending on the grating dispersion and tilt. The maximum range is 23.2 pixels when using the mirror for direct imaging and the minimum is 12.9 pixels when using the 1200-groove/mm grating at its reddest tilt. Accordingly, the control loop gain for the tent mirror (expressed as the FCS image motion in pixels that results from each micron of motion of the tent mirror piezo actuator) must be calibrated for each grating over its full tilt range.* Unfortunately, for some gratings and tilt ranges, the image steering range of the tent mirror is insufficient to fully compensate for the observed image motion in the DEIMOS *Y* axis. In those cases, additional range is provided by using the grating tilt mechanisms.

3.3.3. Grating tilt mechanisms

The two sliders that carry gratings each contain a tilt mechanism with a range of nearly 40°. Each mechanism is driven by a servo motor via a multi-stage friction drive that provides nearly backlash-free positioning. A Gurley incremental encoder is directly coupled on-axis to the tilt axis of each mechanism via an anti-torque arm mechanism and provides a tilt angle resolution of 1.44 arc-seconds per encoder count. This translates to an average image-steering resolution of 0.3 pixel on the detector.

However, due to high-frequency non-linearities in the Gurley encoder,[10] the effective image steering motion on the detector varies between 0.2 and 0.4 pixel per encoder count. Because of this non-linearity and the significantly coarser step size of the Gurley encoder as compared to the tent mirror piezo actuator, the grating tilt mechanism is only used for image steering whenever the piezo actuator approaches one of its limits of travel. When that occurs, any in-progress exposure is paused briefly by closing the shutter; the tent mirror is then driven back to near the center of its range of travel, and the grating is tilted to compensate for the image motion induced by the re-centering of the tent mirror. The shutter is then re-opened and the exposure resumed.

3.3.4. Dewar translation stage

A translation stage within the dewar moves the position of the science CCD mosaic (and the attached FCS CCDs) in the DEIMOS *X* coordinate, i.e., perpendicular to the dispersion (see Fig. 7). The stage is driven through a vacuum coupling via a servo-motor driven leadscrew with a 1 mm pitch. The lead screw is attached to a 4:1 mechanical lever built into the flex stage to further increase the resolution. Stage position is encoded via a 2000-count per revolution encoder directly coupled to the servo motor, which provides an effective resolution of 0.01 pixel of image motion per encoder count. This stage provides an image steering range of 26.4 pixels.

However, since no linear encoder is mounted to the stage, the stage position cannot be measured directly. Accordingly, the accuracy of the stage position is degraded by any backlash or non-linearities in the leadscrew

*This calibration is also fiber specific. There are a pair of FCS fibers at each edge of the slit mask (see Fig. 5), with each pair illuminating one of the two FCS CCDs. Because the two fibers in a given pair are slightly offset from each other in DEIMOS *Y*, the spectrum generated by each one is offset in wavelength from the spectrum generated by the other (see Sect. 3.3.1). As a result, a slightly different tent mirror gain must be used when deriving FCS corrections from one spectrum versus the other. For example, using the 1200-groove/mm grating at a tilt of 8300 Å, a tent mirror gain of 1.502 pixel/micron is used for the spectrum generated by one fiber of the pair while a gain of 1.555 pixel/micron is used for the other; this corresponds to a gain difference of 3.5%. Accordingly, if multi-spot cross-correlation methods are used to derive FCS corrections, such correlations must be applied individually to each spectrum rather than to the full FCS image from each FCS CCD.

mechanism or vacuum coupling. Further, while the mechanism includes a pre-load, that pre-load is insufficient to compensate fully for the weight of this stage. As a result, the backlash characteristics of this stage vary with the position angle of the instrument. These variations will need to be measured and software corrections applied in the FCS control loop in order to achieve optimal positioning accuracy for this stage.

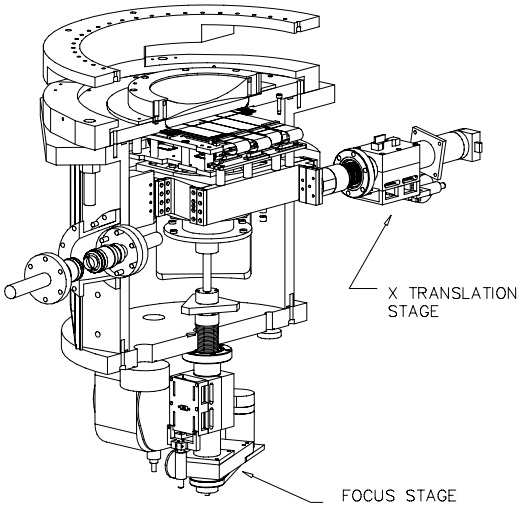

Figure 7. Dewar translation stage

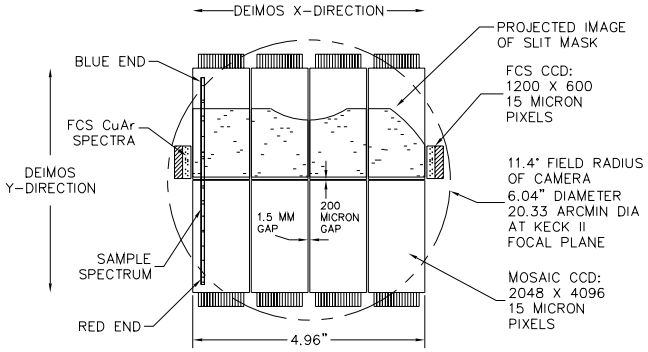

Figure 8. FCS CCDs and science CCD mosaic

3.3.5. FCS CCDs and controller electronics

A 600 row by 1200 column FCS CCD is mounted on each side ($-X$ and $+X$) of the DEIMOS mosaic (see Fig. 8). These CCDs were designed by the UCO/Lick Observatory Detector Laboratory and fabricated under a partnership with Orbit Semiconductor. These devices are unthinned, front-side illuminated, and have 15 micron pixels (the same pixel size as on the science mosaic CCDs). They are mounted parfocal with the science CCD mosaic and are rigidly mounted to the same backplane so as to minimize any flexure of the FCS CCDs relative to the science CCD mosaic.

While these devices are designed to operate in frame transfer mode, we have not yet fully implemented that capability. However, to support the future implementation of frame transfer readout, the dewar and the FCS CCD controller have been wired to provide separate parallel clocks to the upper and lower halves of the FCS CCDs, and the FCS fibers have been aligned so that the images or spectra they generate fall on the half of the FCS CCDs farthest from the serial register. When fully implemented, frame transfer readout will enable more frequent FCS updates and consequently tighter control of image position.

The FCS CCD controller electronics are implemented using the same type of San Diego State University (SDSU) second generation controller boards[11] as are used for the science mosaic CCD controller.[12] However, the FCS CCD controller and the science mosaic controller use completely independent hardware and software, and each subsystem can be run autonomously. Having two independent systems simplified debugging and provided greater flexibility in scheduling activities during assembly and test of the instrument. Electronic cross-talk between these two separate systems (whose CCDs are co-resident in the same dewar) is not an issue since the times at which they read out are mutually exclusive: the FCS CCDs are read out only during the course of an exposure when the shutter is open, while the science mosaic CCDs are read out only at the end of the exposure when the shutter is closed. Thus, there was no need to synchronize the clocks of these two subsystems.

3.4. Measuring flexure

The DEIMOS mechanical design had a goal of limiting total flexure-induced image motion on the detector to 2.5 pixels rms or less in each detector axis or approximately 6 pixels peak-to-peak. Extensive finite element analyses of the main structure suggested that this goal was feasible. Accordingly, the FCS was designed with a compensation range of about 20 pixels in each axis so as to provide more than adequate correction capability.

The initial flexure tests on the assembled spectrograph measured image motions nearly twice as large as the compensation range of the FCS tent mirror and dewar translation stage mechanisms. Analysis indicated that a significant portion of this motion was the result of flexure in the grating support structure, which was stiffened. Loose elements in the DEIMOS camera were found to be an additional major source of image motion. Using an innovative technique developed by Phillips, the offending elements were identified and largely corrected.[13]

Subsequent flexure tests indicated that image motion had been significantly reduced and was now within the compensation range of the dewar translation stage (DEIMOS X axis) in all cases. In the DEIMOS Y-axis (the dispersion direction), the amount of flexure depended on the observing mode. In direct imaging mode, flexure-induced image motion had been reduced within the compensation of the tent mirror mechanism, while in the spectroscopic mode, such motion still exceeded the tent mirror range by several pixels. Additional Y-axis compensation range was then added by utilizing the grating tilt mechanisms as part of the FCS control loop.

Fig. 9 shows the flexure-induced image motion for one of the two sliders (slider 3) that hold the gratings (the results for the other grating slider are similar). Fig. 10 shows the corresponding flexure-induced image motion for the slider that holds the direct imaging mirror. Both figures are plotted within a 20 by 20 pixel grid. These flexure curves were obtained by rotating DEIMOS continuously through 730 degrees of rotation (i.e., from one rotation limit to the other) at a speed of 0.05 degrees/second, first rotating in the forward direction and then rotating in reverse. While DEIMOS was rotating, images were obtained from the FCS CCDs about every 2 degrees of rotation. For each of these images, the centroid of a specific reference spot was measured and plotted. The points obtained while rotating in the forward direction are connected by solid lines, while those obtained in the reverse direction are connected by dotted lines. The flexure pattern is not perfectly repeatable over each rotation, although there is more consistancy between the curves for rotations in the same direction.

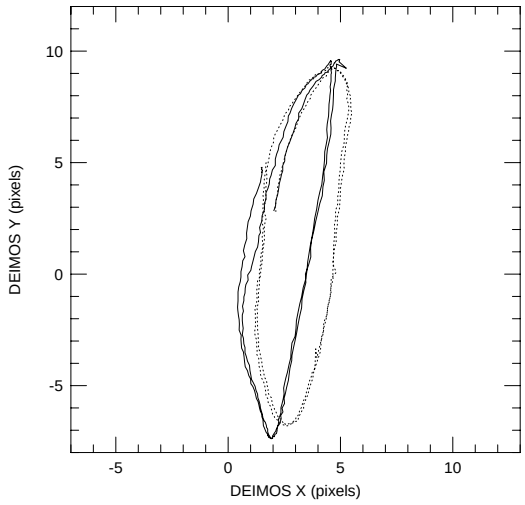

Figure 9. Flexure using a grating slider

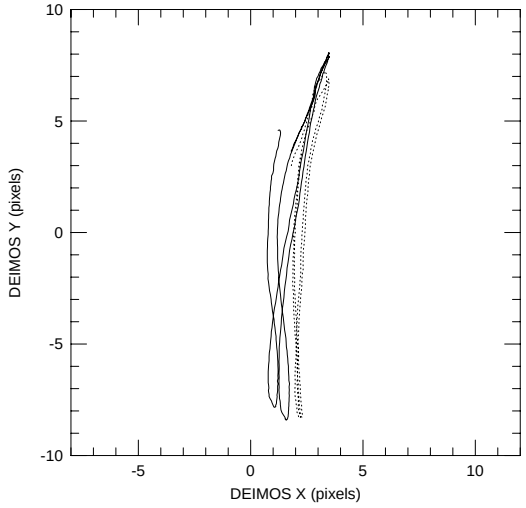

Figure 10. Flexure using direct imaging slider

3.5. Modeling

The flexure-induced image motions shown in Figs. 9 and 10 can be approximated using a model of the form:

$$X(\theta) = a_0 + a_1 \sin(\theta + a_2) \tag{3}$$

$$Y(\theta) = b_0 + b_1 \sin(\theta + b_2), \tag{4}$$

where X corresponds to the predicted position of the reference feature in the X (or column) axis of the CCD, Y to the predicted position in the Y (row) axis, θ to the DEIMOS physical position angle, and a_i and b_i are the corresponding coefficients obtained from a least square fit of the data to the model. The flexure results for each combination of slider and grating are fitted separately.

While one might argue that such a model is unnecessary because the DEIMOS FCS is a closed-loop system, there are circumstances when it is useful to operate the DEIMOS FCS as an open-loop system like the one used by ESI. First, the DEIMOS FCS closed-loop system is essentially blind whenever the shutter in front of the dewar is closed, as is the case when the science mosaic is being erased or reading out, or when the telescope is slewing to a new position in the sky. Second, because of the exposure and readout times for the FCS CCDs, the DEIMOS FCS can only only make closed-loop corrections a few times per minute. When tracking an object across a portion of the sky where the physical position angle of the instrument is changing rapidly (e.g., at meridian crossing close to zenith), the infrequent closed-loop correction rate of the DEIMOS FCS may be insufficient to meet the image stability specification.

In such situations, a hybrid open/closed-loop correction scheme will likely provide better image stability. The open-loop correction derived from the flexure model will provide an approximate local correction that will be applied in between closed-loop corrections. The closed loop corrections can then be used both to trim up the image position and to adjust the zero points (but not the shape) of the flexure model so as to account for shifts due to mechanical hysteresis or variations in the clamping of the sliders to the rigid mounting box.

3.6. Operational Issues

3.6.1. Scattered FCS light

A consideration in designing the FCS system is the amount of scattered FCS light that escapes over onto the science detector[†]. The FCS light must be quite bright compared to the science spectra, as good S/N for centroiding must be obtained in exposure times as short as 10 s. The density of lines must also be high so that lines are available with all dispersions and grating tilts. As we have noted, the latter requirement led to our choice of a CuAr lamp, with its very rich spectrum of lines. However, a drawback of the CuAr spectrum, as shown in Fig. 6, is that the lines in the blue are roughly 30 times dimmer than the brightest lines in the red. If a bare lamp with no color-balancing filter is used, making the blue lines bright enough requires turning the lamp brightness so high that the red lines are tremendously bright, with the result that too much scattered FCS light spills out onto the science detector.

Our first configuration ran the FCS light source at high intensity and with no filter. We estimated that 5% of the light falling onto each FCS detector was scattered onto the portions of the science detector nearest to it. The scattered light intensity in 1000 s near the FCS detectors was a few hundred photons per pixel, clearly unacceptable.

The solution was to turn down the overall light intensity, which we did by misaiming the collimated CuAr light beam shining on the ends of the FCS fibers, and inserting a color-balancing filter to kill the red light. The Schott BG38 and BG40 glasses both absorb red light and pass blue light, with the transition occurring at about 5800 Å, well matched to the break in the CuAr spectrum. BG38 (2 mm) is preferred because its red rejection is about a factor of two higher than BG40 (1 mm). Use of BG38 yields a lamp brightness in the blue that is just bright enough for centroiding, with virtually no scattered light visible on the science detector[‡]

To further reduce scattered light, some care should be taken to baffle the FCS detectors so that the unused portions of the CuAr spectrum (at higher and lower wavelengths) do not enter the dewar. We achieved this by mounting a separate opaque baffle between the field flattener and the dewar window. This baffle was irregularly shaped with openings for the FCS CCD detectors but intercepted light in the spectrum to the red and blue of those detectors. The same baffle also shielded light that had been scattering off the inner lip of the dewar window in the corners of the field of view. A drawback to the present scheme is that light is somewhat out of focus as it passes by the edge of the baffle (the beam is about 0.3 inch in diameter there), and thus the baffle has to be somewhat oversized. However, there was little room for it in front of the CCDs inside the dewar, and it seems to be doing a satisfactory job in its present location.

[†]FCS scattered light was avoided in the FCS for the Gemini HROS spectrograph by using an IR FCS light source whose wavelength was within the passband of the spectrograph optics but outside that of the optical CCDs used for science. However, this requires IR FCS sensors.

[‡]Future closed-loop implementations should consider providing remote control of the CuAr lamp intensity so that it can be optimized dynamically for the currently selected grating, grating tilt, and science filter.

3.6.2. CuAr Line Density

The CuAr spectrum provides a rich set of lines over most of the DEIMOS wavelength range of 4000 to 10000 Å. However, between 5220 to 5500 Å, none of the lines is adequately bright in a 10s exposure. When operating in this region using the highest dispersion grating, longer exposure times will be needed to generate lines bright enough to centroid, thus reducing the FCS update rate. In practice, this affects only 100 Å of the tilt range of the 1200-line grating.

In the absence of the hybrid open/closed-loop scheme described earlier, following a telescope slew which results in a large change in instrument physical position angle during a period when the shutter is closed, a given FCS reference spot may have moved as much as 20 pixels from the position at which it was last measured by the FCS. To ensure that the same spot is re-acquired once the shutter is re-opened following the slew, the analysis box used for centroiding should be of order 30 by 30 pixels. In such cases, an FCS reference spot of adequate brightness may prove to be unusable if it is within 30 pixels of another FCS spot of similar brightness, since the centroiding routine could potentially lock onto the wrong spot. Thus, while it is necessary to have a relatively high density of lines to ensure that FCS spots will always be available, too high a density can also prove problematic. This will cease to be a problem if an open-loop model proves able to predict the spot location of each CuAr line at each grating tilt to reasonable accuracy, or if the shutter is left open while slewing.

3.6.3. Centering reference positions within the flexure curve

In its current implementation, the DEIMOS FCS will track the position of a selected spectral feature (or FCS fiber image if in direct imaging mode) on one of the two FCS CCDs; changes in the position of that feature will generate an error signal resulting in updated positions for the tent mirror and dewar translation stage. We refer to this selected feature as the FCS *reference spot*; the FCS CCD pixel coordinates at which the FCS will try to hold that reference spot are denoted as the *reference position*.

Because the uncontrolled flexure-induced image motion is nearly as large as the compensation range of the FCS tent mirror and dewar translation mechanisms, the reference position (which is normally determined during the afternoon when calibration exposures are taken) should be measured only when: (1) those mechanisms have been driven to the center of their respective ranges of travel, (2) any grating tilt offsets are set to zero, *and* (3) the instrument is rotated to a position angle that corresponds to the center of the flexure range for the currently selected slider. Otherwise, if the reference position is measured at an arbitrary instrument position angle or with the FCS mechanisms not properly nulled, the FCS control loop might ultimately lose its lock on the reference spot because it has driven one of those mechanisms to its limit of travel in an attempt to hold that spot at its reference position as the instrument rotates.

3.6.4. Other issues

Other operational issues include calibrating and removing the effects of differential flexure between the four FCS fibers and between those fibers and the slitmask, as well as compensating for focus and transmission/intensity differences between the fibers. While differential flexure is known to be quite small, if not properly handled, the result is to stabilize a reference spot on its FCS CCD while the image on the science CCD mosaic is smeared by an amount comparable to the relative flexure between the FCS reference fiber and the slitmask. Further work is currently in progress to address these issues.

3.7. Preliminary Operating Procedures

During instrument commissioning in July 2002, prototype FCS software was deployed that supports several basic functions that are currently implemented as scripts: *fcszero* rotates DEIMOS to the instrument position angle that corresponds to the center of the DEIMOS Y flexure curve for the currently selected slider and drives the FCS mechanisms to their respective range-of-travel centers; *fcsref* enables the observer to select and record the reference position of the FCS feature that will be used as the reference spot for the current instrument configuration; *fcstrack* enables the FCS control loop so that it will try to hold the reference spot at the reference position whenever the shutter remains open for a sufficient period of time to allow an FCS image to be acquired. (Note that the FCS CCDs and the science mosaic CCDs share a common shutter, which is under the direct control of the science mosaic CCD controller but which can be commanded open for separate FCS exposures.)

During the afternoon, the observer will acquire science-mosaic arc-lamp and flat-field exposures for each of the instrument configurations planned for that night's observing. For each configuration, the observer will first perform the *fcszero* and *fcsref* functions, and then proceed (with the instrument parked at the position angle set by the *fcszero* function) to take the calibration images for that configuration.

During the night, the observer will enable the *fcstrack* function, which will monitor the current instrument configuration. Whenever the configuration changes, the *fcstrack* function will acquire the reference spot that was identified for that configuration during the afternoon calibrations and periodically adjust the FCS mechanisms so that that reference spot is held at its reference position. (If no reference spot was defined for a given configuration, then the FCS becomes idle until another configuration having a defined reference spot is selected.) Thus, science exposures acquired during the night should register with calibration exposures taken during the afternoon.

Because small, slow drifts in image position can occur (due to temperature changes or other position-angle-independent effects) while the instrument is parked at a fixed position angle[§], it would be desirable to leave FCS tracking enabled during the afternoon when calibration exposures are taken. Unfortunately, in many cases this is not currently possible, since some of the calibration sources (e.g., the quartz lamp used for flat fields) scatter significant amounts of stray light onto the FCS CCDs, washing out all but the brightest of the FCS spots. In such cases, these drifts can be partially compensated by periodically turning off the calibration lamps and affording the FCS an opportunity to make a correction by briefly opening the shutter.

Similarly, during the night, when slewing to a new field, the reference spot may have moved many pixels from its last observed position, since the shutter is typically closed (and FCS tracking inhibited) while slewing. In such cases, it may be desirable to open the shutter once the new field is acquired but before starting the science exposure, in order to give the FCS a chance to drive the reference spot back to its reference position first. Implementation of an open-loop correction model may eliminate the need for such actions. Alternatively, this problem can be avoided by leaving the shutter open while slewing so that the FCS will continue to apply corrections. To prevent stray light from very bright objects from entering the camera while slewing, one can either close the hatch or insert a slitmask.

3.8. Preliminary Performance Results

Closed-loop FCS tracking tests have been conducted during the day to determine how well the FCS is able to hold a given reference spot at its reference position for various instrument configurations and rotation rates of the instrument. For example, using the 830-line grating and a rotation rate of 0.05 degrees/second, rms tracking errors were 0.08 pixels in DEIMOS X and 0.33 pixels in DEIMOS Y over two continuous revolutions of the instrument. The large rms error in DEIMOS Y is the result of non-optimal offsetting of the grating tilt during each tent mirror re-centering sequence (see Sect. 3.3.3). If one excludes the points corresponding to images taken immediately following such a re-centering sequence, the rms tracking error in DEIMOS Y drops to 0.20 pixels.

Using the prototype FCS scripts, FCS-stabilized science exposures were obtained during the first DEIMOS science run in July 2002. Although this sequence of exposures was not intended to be a systematic test of the FCS, it does provide some partial measures of two aspects of FCS performance. First, how well centered are the various portions of the science image during a long observation that consists of several exposures? Second, how well is each science exposure aligned with its corresponding flat-field (and internal arc) image taken during the afternoon?

3.8.1. Centration of science images during a long observation

Hour-long spectroscopic observations for three science fields were analyzed. (The change in DEIMOS physical position angle during each of these observations ranged from 23° to 56°.) Each observation consisted of four 15-minute exposures. The locations of nine specific image features (night sky lines in the multislit spectra) were

[§]The FCS was used to monitor image motion while DEIMOS was parked at a fixed position angle and all DEIMOS stages held at fixed positions. Over an interval of 75 minutes, image motion of 0.21 pixels in X and 0.16 pixels in Y was observed. Over a 250 minute interval, the observed motions were 0.36 pixels in X and 0.26 pixels in Y.

compared between the first and last exposures within each observation. These nine features were spaced across the length and width of the mosaic: three short-slit spectra were selected at low, medium, and high X locations along the slit, and within each spectrum three features were chosen at blue, middle, and red wavelengths. Mean rms residuals (averaged over the mosaic) for each of the three observations varied between 0.12 and 0.52 pixels in DEIMOS X and between 0.10 and 0.39 pixels in DEIMOS Y.

The FCS corrections in this data set were derived from a single reference spot on FCS CCD 1. One of the measured features on the science mosaic is very close to this reference spot, and the motions observed for this feature are typically only 0.1 pixel. This suggests that: 1) any flexure between the FCS reference spot fiber and the science mosaic is small, 2) the motion of that FCS spot was representative of the nearby spots on the science mosaic, and 3) the reference spot was held within 0.1 pixel of its reference position during these observations.

We predict that if two reference spots had been used (one on FCS CCD 1 and the other on FCS CCD 2) to derive these FCS corrections, the mean image motion for these observations would have been reduced, and that the corresponding mean rms residuals would have been of order 0.3 pixel in DEIMOS X and Y.

3.8.2. Alignment of science exposures with flat fields

The edge positions of the afternoon flat-field spectra were compared to the edge positions of night-sky emission lines from the nighttime observations. This method measures image motion only in DEIMOS X. (The change in DEIMOS physical position angle between the afternoon and nighttime observations ranged from 17° to 54°.) For the three observations analyzed, image alignment errors were 0.5 pixel or less.

3.9. Further Plans

Considerable work remains to optimize the performance of the FCS and repackage it as a turnkey system that imposes minimal extra effort on the observer. Now that more urgent commissioning tasks have been completed, we hope to undertake a more systematic analysis of FCS performance. We also hope to improve FCS performance by: implementing a hybrid open/closed-loop control strategy; developing an archive of reference spot positions for all configurations; adding the capability to track multiple reference spots simultaneously (and on both FCS CCDs) to improve tracking accuracy (and cosmic ray rejection) and to provide online measurement of image rotation and focus stability; improving compensation for focus variations, intensity variations, and differential flexure (if any) between fibers; and implementing frame transfer readout in order to speed up the closed-loop correction cycle.

4. CONCLUSION

Two important design and implementation issues proved common to the flexure compensation systems for ESI and DEIMOS. First, there was a tendency for our finite element analyses (FEA) to under-predict the overall instrument flexure because they were not sufficiently detailed. We had incorrectly assumed that the macro structure of the instrument would be the dominant source of flexure. Accordingly, our FEA did not attempt to model many of the individual substructures because their flexure was not thought to be significant and because they were considered too complex to model. However, these substructures proved to be a major source of flexure. In the case of DEIMOS, these overly optimistic predictions resulted in range-of-travel specifications for the active mechanisms that were barely able to handle the actual flexure. If these mechanisms had a greater range of travel, the FCS control loop and operational procedures for DEIMOS could have been greatly simplified.

Second, in both instruments, the camera designs are extremely sensitive to minute mechanical tolerances. Accordingly, loose elements in the camera had a profound effect on observed image motion and confounded our early attempts to measure flexure of the instrument structures. This resulted in significant delays and costs during instrument integration. These problems might be reduced in future instruments by conducting more extensive sensitivity analyses of the camera assembly tolerances, more careful checking of the details of the assembly process, and by developing better methods for testing the camera to detect and correct such loose elements prior to integration with the spectrograph.

Despite these difficulties, both the ESI and DEIMOS FCS have demonstrated that they are able to reduce image motion significantly and reliably and thereby greatly improve the overall image quality and calibration accuracy of the data collected by these instruments.

ACKNOWLEDGMENTS

For the commissioning of the ESI FCS, we thank Teresa Chelminiak, Bob Goodrich, Gary Puniwai, and Ron Quick of Keck Observatory for their assistance in collecting the closed-dome flexure tests. Goodrich also contributed significantly to the reduction and analysis of the ESI flexure data. Jim Burrous (deceased) helped to develop the low-level motor control software for all of the ESI stages, including the collimator actuators. For the commissioning of the DEIMOS FCS, we thank Gabrelle Saurage, Cinthia Wilburn, Ron Quick, Joel Aycock and Greg Wirth of Keck Observatory for their assistance. We also acknowledge Elizabeth Chock, Jon Chock, Al Conrad, and Julia Simmons for their assistance in commissioning the overall software for both the ESI and DEIMOS spectrographs. Thanks also to Vernon Wallace for assistance in generating the figures for the DEIMOS portion of this paper.

DEIMOS was started in 1992 with a Facilities and Instrumentation grant from the National Science Foundation (ARI92-14621) in the amount of $1.79 million. The California Association for Research in Astronomy has so far contributed approximately $7.2 million directly to the project, not including the additional costs of CARA liaison and alterations that were needed for the Keck 2 telescope. UCO/Lick Observatory has contributed over $1 million so far in manpower.

REFERENCES

1. D. D. Walker and P. D'Arrigo, "On the stability of Cassegrain spectrographs," *Mon. Not. R. Astron. Soc.* **281**, pp. 673–678, 1996.
2. H. Nicklas *et al.*, "Image motion and flexure compensation for the FORS spectrograph," in *Optical Astronomical Instrumentation*, S. D'Odorico, ed., *Proc. SPIE* **3355**, pp. 93–104, 1998.
3. W. Seifert *et al.*, "Commissioning of the FORS instruments at the ESO VLT," in *Optical and IR Telescope Instrumentation and Detectors*, M. Iye, ed., *Proc. SPIE* **4008**, pp. 96–103, 2000.
4. P. D'Arrigo, R. Bingham, A. Charalambous, K. Saber-Sheikh, and T. Savidge, "Active Flexure Compensation for the HROS Spectrograph," in *Optical and IR Telescope Instrumentation and Detectors*, M. Iye, ed., *Proc. SPIE* **4008**, pp. 861–865, 2000.
5. K. Szeto, R. Murowinski, S. Roberts, and L. Saddlemeyer, "Gemini Multi-Object Spectrograph - a Flexure Critical Design," in *Optical Astronomical Instrumentation*, S. D'Odorico, ed., *Proc. SPIE* **3355**, pp. 297–306, 1998.
6. B. C. Bigelow, A. M. Dressler, S. A. Shectman, and H. W. Epps, "IMACS: The multi-object spectrograph and imager for the Magellan I telescope," in *Optical Astronomical Instrumentation*, S. D'Odorico, ed., *Proc. SPIE* **3355**, pp. 225–231, 1998.
7. A. Sheinis *et al.*, "ESI, a new Keck Observatory Echellette Spectrograph and Imager," *P.A.S.P.* **114**, pp. 851–865, 2002.
8. E. James, D. Cowley, S. M. Faber, D. Hilyard, and C. Osborne, "Design update of DEIMOS, a wide field, faint object spectrograph," in *Optical Astronomical Instrumentation*, S. D'Odorico, ed., *Proc. SPIE* **3355**, pp. 70–80, 1998.
9. R. Kibrick, J. Miller, J. Nelson, M. Radovan, A. Sheinis, and B. Sutin, "Active flexure compensation software for the Echellette Spectrograph and Imager on Keck II," in *Advanced Telescope and Instrumentation Control Software*, H. Lewis, ed., *Proc. SPIE* **4009**, pp. 262–273, 2000.
10. L. Robinson, R. Kibrick, D. Cowley, and J. Osborne, "Tests of incremental rotary encoders," in *Telescope Control Systems II*, H. Lewis, ed., *Proc. SPIE* **3112**, pp. 42–49, 1997.
11. R. Leach, F. Beale, and J. Eriksen, "New generation CCD controller requirements and an example: the San Diego State University generation II controller," in *Optical Astronomical Instrumentation*, S. D'Odorico, ed., *Proc. SPIE* **3355**, pp. 512–519, 1998.
12. C. Wright, R. Kibrick, and B. Alcott, "CCD imaging systems for DEIMOS," in *Instrument Design and Performance for Optical/Infrared Ground-Based Telescope*, M. Iye, ed., *Proc. SPIE* **4841**, 2002.
13. S. Faber *et al.*, "DEIMOS spectrograph for the Keck 2 telescope: integration and testing," in *Instrument Design and Performance for Optical/Infrared Ground-Based Telescope*, M. Iye, ed., *Proc. SPIE* **4841**, 2002.